# NUMERICAL INVESTIGATION OF THE EFFECTS OF SWEEP ANGLE ON THE BOUNDARY-LAYER TRANSITION IN HIGH SPEED FLIGHT

S Shahpar

The Manchester School of Engineering *(Aerospace Division)*
University of Manchester, UK.

## Abstract

The work presented here is an initial foray into a problem concerning the steady, laminar flow on hypersonic swept wings. Of particular interest is the computations of the cross-flow profiles which are a source of laminar to turbulent flow transition near the leading edge of swept wings. A single march Infinite Swept Navier-Stokes code (ISPNS) has been developed to compute the flow field from which certain characteristics of the boundary-layer profiles are quantified to indicate any possible trends. It is hoped that this data, backed by experimental measurements, can be used to produce empirical relations to estimate the transition location for high speed cross-flow dominated problems. As part of this study the effects of varying the free stream Mach number, unit Reynolds number, leading edge sweep, and angle of attack on the cross-flow profiles have been considered in detail and the results are presented herein.

## Nomenclature

| | |
|---|---|
| $c$ | Cross-flow velocity |
| C1, C2 | Arnal's correlation parameters[9] |
| $Cp$ | heat capacity at constant pressure |
| **E**, **F**, **G** | Vector fluxes given by Eqn (1) |
| $H_w$, $H_o$ | Wall enthalpy, total enthalpy |
| $H_{cf}$ | Cross flow shape factor |
| $H_{11}$ | Three-dimensional shape factor |
| $J$ | Transformation Jacobian |
| $L$ | Typical length (chord of the delta wing) |
| $M_\infty$ | Free stream Mach number |
| $p$ | Pressure |
| $Pr$ | Prandtl number, 0.72 |
| $\dot{q}_w$ | Heat transfer rate at the wall |
| $Q_\infty$, $Q_e$ | Free stream velocity and streamwise local inviscid velocity |
| $Re_c$ | Cross flow Reynolds number, Eqn (11) |
| $Re_e$ | Reynolds number at the edge of the boundary-layer |
| $\overline{Re}_\infty$ | Free stream unit Reynolds number |
| $R_{LE}$ | Leading edge radius |
| $St$ | Stanton number, Eqn (14) |
| $t$ | Time |
| $T$ | Temperature |
| $u$, $v$, $w$ | Cartesian velocity components |
| **U** | Vector of conservative variables, Eqn (1) |
| $\alpha$, $\alpha_e$ | angle of attack, effective $\alpha$ |
| $\beta$ | maximum cross flow velocity/$Q_e$ |
| $\gamma$ | ratio of specific heats, 1.4 |
| $\delta$ | boundary layer thickness |
| $\delta^*$ | displacement thickness |
| $\delta_{i,j}$ | Kronecker delta |
| $\Delta$ | step size increment |
| $\zeta$, $\eta$, $\xi$ | Spanwise, normal to the wall and chordwise directions |
| $\Lambda$ | Sweep angle |
| $\mu$ | Viscosity |
| $\nu$ | Kinematic viscosity |
| $\rho$ | Density |
| $\sigma$ | Safety factor, slightly less than unity |
| $\tau_{xy}$, $\tau_{xx}$ | Shear stress in x-y-plane, direct stress in x-direction |
| $\phi$ | local flow angle |
| $\chi$ | Cross flow Reynolds number, Eqn (9) |
| $\omega$ | Splitting parameter for chordwise pressure gradient |

## 1. Introduction

Interest in supersonic laminar flow control (LFC) is increasing because of the possible large gains in performance, range and lower surface temperature for high speed transport aircraft[1]. These advantages would lead to a reduction in fuel consumption and therefore to more economical and environmentally friendly aircraft[2]. The development and application of laminar flow control (LFC) techniques to swept wings requires a detailed understanding of the effects of "spanwise contamination" and the "cross-flow vortices" on boundary layer stability and transition in the leading edge region. These two mechanisms, which may cause transition in the leading-edge regions of swept wings, have been extensively studied for subsonic flows[3–5]. The problem of spanwise turbulent contamination along the attachment line of swept wings was recognised in the 1960's. Critical values of the attachment line momentum thickness Reynolds number $\overline{R}_*$ were found to be about 100 in the presence

of large upstream disturbances and about 240 with all disturbances minimized[3]. The phenomena of leading edge contamination has also been extensively studied by Poll[4,5] at subsonic speed and, recently, his attachment line transition correlations have been extended to more general cases involving compressibility and heat transfer[6]. Poll studied the response of the attachment line boundary layer to trip wires of different diameters fixed to the surface and normal to the wing leading edge. The variation of critical Reynolds number with roughness height could then be correlated with a new parameter to predict the onset of attachment line transition. In the absence of any tripping or surface roughness, fully laminar flows can be achieved for values of up to 650. Increasing the trip wire diameter reduces $\overline{R}_*$ in the "critical" range up to a "fully effective" trip size where $\overline{R}_*$ is about 245.

In the absence of "spanwise contamination" on the attachment line, transition can still occur near the leading edge of swept wings due to cross-flow instability. The aerodynamic efficiency of wings that have been or are currently being designed for supersonic/hypersonic aerospace planes requires them to be highly swept and relatively thin. However, the viscous-inviscid interactions over a swept wing with a sharp leading edge would lead to a shock wave being generated and a pressure field being induced. For swept wings, the combination of an external pressure gradient and a viscous layer (across which the pressure is almost constant but the momentum is lower) would always lead to generation of cross-flow, i.e. the development of a velocity component inside the boundary layer that is perpendicular to the local inviscid-flow velocity vector. All cross-flow velocity profiles have zero velocity at the wall and tend to zero velocity at the viscous layer edge. In the vicinity of a swept leading edge the profile has a "⊃" shape that has a single maximum and an inflection point (a condition that is known to be dynamically unstable), see figure 1.

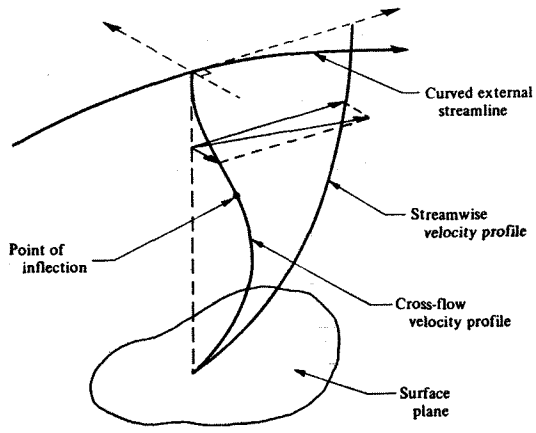


Figure 1 Schematic of velocity components within a swept wing boundary layer

This phenomena was first observed in the flight experiment of Gray[7] as regularly spaced streaks caused by variations in mass transfer from surface coatings. The streaks are formed by co-rotating vortices, in the shape of "cat's eyes" resulting from the inflectional instability of the cross-flow boundary-layer profiles.

In the initial phase of this investigation, a general, non-interactive infinite swept Navier-Stokes (ISPNS) code has been developed to predict the steady hypersonic flows over a plate of infinite span with a sharp leading edge. The equations are solved using an implicit, approximate-factorisation, finite difference scheme which is second-order accurate in the normal to the wall and in the cross-flow directions. The effects of varying the sweep angle, the free stream unit Reynolds number, Mach number and angle of attack are presented. It must be pointed out that the purpose of the presented parametric computational study has been to reveal any trends that might exist. The basic state numerical result will be later manipulated with the aid of experimental data and/or stability analyses to produce empirical relations similar to those mentioned above for the boundary-layer instability due to "spanwise contamination" of attachment line. It is hoped that these new empirical relations can be used to predict the position of transition location for high speed cross-flow dominated flows.

## 1.1 Geometry

A typical delta wing with sweep angle of $\Lambda$ is shown in figure 2. For typical wings, sweep angles are unlikely to exceed 80° and for free stream Mach numbers in excess of 5, i.e. hypersonic flow, the Mach number in a plane drawn normal to the leading edge will be in excess of unity. This is also true for moderate Mach numbers of 2-2.5 with sweep angles of approximately 60°, categories to which most fighter aircraft, and current and future supersonic transport aircrafts belong to. This being the case, two limiting cases of sharp and blunt leading edges can be considered.

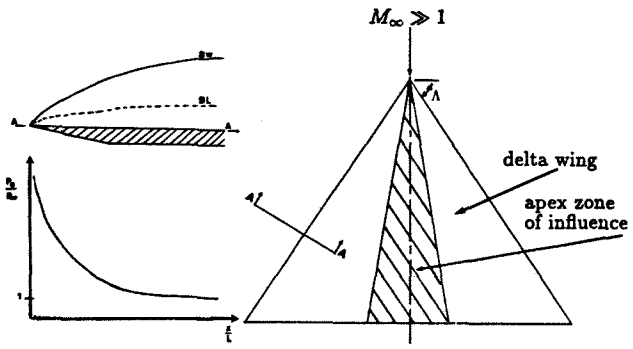


Figure 2 Typical planform and normal to leading edge section details

In the initial phase of this research the limiting case where the leading edge is sharp is considered. Moreover, away from the apex of the wing the leading edge region will be unaware of the details of the delta wing planform and the flow will be locally "infinitely swept". This implies that there are no pressure or velocity gradients in the spanwise direction and the bow shock wave, detached or attached, has to be parallel to the leading edge. The main flow features are shown in figure 2.

## 2. Governing equations

### 2.1. Unsteady Navier-Stokes equations

The compressible viscous flow equations can be written in strong conservation and general coordinate form, where the $\xi$-direction is along the chord and the $\zeta$-direction is along the span of the delta wing, as shown in figure 3, without body forces or external heat and mass transfer as

$$\frac{\partial \overline{\mathbf{U}}}{\partial t} + \frac{\partial \overline{\mathbf{E}}}{\partial \xi} + \frac{\partial \overline{\mathbf{F}}}{\partial \eta} + \frac{\partial \overline{\mathbf{G}}}{\partial \zeta} = 0 \qquad (1)$$

where

$$\mathbf{U} = \begin{bmatrix} \rho \\ \rho u \\ \rho v \\ \rho w \\ \bar{e} \end{bmatrix};$$

$$\mathbf{E} = \begin{bmatrix} \rho u \\ p + \rho u^2 - \tau_{xx} \\ \rho uv - \tau_{xy} \\ \rho uw - \tau_{xz} \\ (\bar{e}+p)u - u\tau_{xx} - v\tau_{xy} - w\tau_{xz} + q_x \end{bmatrix};$$

$$\mathbf{F} = \begin{bmatrix} \rho v \\ \rho uv - \tau_{xy} \\ p + \rho v^2 - \tau_{yy} \\ \rho uw - \tau_{yz} \\ (\bar{e}+p)v - u\tau_{xy} - v\tau_{yy} - w\tau_{yz} + q_y \end{bmatrix};$$

$$\mathbf{G} = \begin{bmatrix} \rho w \\ \rho uw - \tau_{xz} \\ \rho vw - \tau_{yz} \\ p + \rho w^2 - \tau_{zz} \\ (\bar{e}+p)w - u\tau_{xz} - v\tau_{yz} - w\tau_{zz} + q_z \end{bmatrix};$$

$$\bar{e} = \left[\frac{p}{(\gamma-1)} + \frac{1}{2}\rho(u^2+v^2+w^2)\right];$$

$$\overline{\mathbf{U}} = \frac{\mathbf{U}}{\mathbf{J}},$$

$$\overline{\mathbf{E}} = \frac{\mathbf{E}\xi_x + \mathbf{F}\xi_y + \mathbf{G}\xi_z}{J},$$

$$\overline{\mathbf{F}} = \frac{\mathbf{E}\eta_x + \mathbf{F}\eta_y + \mathbf{G}\eta_z}{J},$$

$$\overline{\mathbf{G}} = \frac{\mathbf{E}\zeta_x + \mathbf{F}\zeta_y + \mathbf{G}\zeta_z}{J}.$$

$J$ is the transfer Jacobian of the general coordinate system, i.e. $J = \left|\frac{\partial(\xi,\eta,\zeta)}{\partial(x,y,z)}\right|$, and

$$\tau_{ij} = \frac{\mu}{Re_{\infty,n}}\left[\left(\frac{\partial u_i}{\partial x_j} + \frac{\partial u_j}{\partial x_i}\right) - \frac{2}{3}\frac{\partial u_k}{\partial x_k}\delta_{ij}\right] (i,j,k = 1,2,3),$$

$$q_i = \frac{-\gamma\mu}{(\gamma-1)Re_{\infty,n}Pr}\frac{\partial T}{\partial x_i} \quad (i = 1,2,3).$$

In these equations, $p, \rho$ and $T$ are non-dimensional pressure, density and temperature respectively and $\bar{e}$ is the total energy per unit volume. The Prandtl number, Pr, is assumed to be 0.72 and $\gamma = 1.4$. The coefficient of molecular viscosity $\mu$ is assumed to vary with temperature according to Sutherland's law:

$$\mu(T) = \frac{(\gamma M^2_{\infty,n} T)^{\frac{3}{2}}}{(\gamma M^2_{\infty,n} T\tilde{T}_\infty + 110.4)}(\tilde{T}_\infty + 110.4) \qquad (2)$$

All quantities in the above equations were non-dimensionalised with respect to the free stream values and the velocity normal to the leading edge. For example,

$\rho = \frac{\tilde{\rho}}{\tilde{\rho}_\infty}$, $p = \frac{\tilde{p}}{\tilde{\rho}_\infty(\tilde{Q}_\infty \cos\Lambda)^2}$, $T = \frac{\tilde{T}}{\gamma M^2_{\infty,n}\tilde{T}_\infty}$,
$W_\infty = \tan\Lambda$, and $M_{\infty,n} = M_\infty \cos\Lambda$ .

### 2.2 The infinite swept parabolized Navier-Stokes Eqns

The parabolized Navier-Stokes (PNS) equations are a subset of the full Navier-Stokes equations obtained by eliminating the unsteady terms and neglecting the contribution of viscous derivatives in the marching direction i.e. along the surface and normal to the leading edge. The resulting equation set is valid in both the inviscid and viscous regions of the flow with all the effects of second-order boundary-layer theory included. Thus the PNS equations are particularly well suited for calculating flow fields where there is interaction between the viscous and the inviscid regions of the flow. Eliminating $\partial/\partial t$ and $\partial/\partial\xi$ in the viscous terms and additionally, as mentioned in section 1.1, using the infinite swept assumption which implies that $\zeta$-derivatives are zero, the ISPNS equations become

$$\frac{\partial \overline{\mathbf{E}}}{\partial \xi} + \frac{\partial \overline{\mathbf{F}}}{\partial \eta} = 0 \qquad (3)$$

where

$\overline{\mathbf{E}} = \frac{1}{J}(\xi_x\mathbf{E} + \xi_y\mathbf{F})$, and $\overline{\mathbf{F}} = \frac{1}{J}(\eta_x\mathbf{E} + \eta_y\mathbf{F})$.

Note that the vector $\overline{\mathbf{E}}$ still has 5 components, and there is strong coupling between the spanwise momentum equation and the other two chordwise and normal

momentum equations. For example, the shear stress in the yz-plane, $\tau_{yz}$, has a non-zero value (i.e. $\frac{\mu}{Re_\infty}\frac{\partial w}{\partial \eta}$) which appears in the energy equation of $\overline{\mathbf{F}}$ as $w\tau_{yz}$.

The flux vector $\overline{\mathbf{E}}$ in Eqn (3) includes the pressure and, therefore, the streamwise pressure gradient appears in $\partial\overline{\mathbf{E}}/\partial\xi$ with no modifications to the streamwise pressure gradient within the subsonic regions. The equations are elliptic in these regions and thus the downstream flowfield influences the upstream flow. Therefore, a space marching procedure is not well posed unless this elliptic influence is suppressed. If a marching procedure is used, exponential growth or decay in the solution near the surface can occur which is known as the 'departure solution'. To overcome this difficulty, the streamwise pressure gradient is modified in the subsonic regions. One approach[13] is to split the inviscid flux vector $\overline{\mathbf{E}}$ as

$$\overline{\mathbf{E}}^* = \overline{\mathbf{E}} - \overline{\mathbf{P}} \tag{4}$$

where,

$$\overline{\mathbf{E}}^* = [\rho u,\ \rho u^2 + \omega p,\ \rho uv,\ \rho uw,\ (\bar{e}+p)u]^T/J,$$

$$\overline{\mathbf{P}} = [0,\ (1-\omega)p,\ 0,\ 0,\ 0]^T/J.$$

In the supersonic position of the flow field, $\omega$ is unity and no modification of the pressure gradient is required, but in the subsonic regions of the flow a fraction of the pressure gradient term, $\omega\partial p/\partial\xi$, is retained and the remainder $(1-\omega)\partial p/\partial\xi$ is either omitted or evaluated explicitly on the right hand side using a backward difference formula. An eigenvalue stability analysis indicates that for stability

$$\omega = \min\left[1,\ \frac{\sigma\gamma M_\xi^2}{1+(\gamma-1)M_\xi^2}\right] \tag{5}$$

where $M_\xi$ is the Mach number in the $\xi$-direction, and $\sigma$ is a safety factor included to provide for non-linearities not accounted for in the stability analysis.

## 3. Method of solution

Equation (3) is solved using an efficient, implicit, non-iterative method which is second-order accurate in the normal and cross-flow directions and first order in the marching ($\xi$ ) direction. The quasi-linearised form of the equation (3) for an infinite swept flow where $\Delta\xi$ is constant is

$$\left[\frac{\partial\overline{\mathbf{E}}^*}{\partial\overline{\mathbf{U}}} + \Delta\xi.\frac{\partial}{\partial\eta}\left(\frac{\partial\overline{F}}{\partial\overline{\mathbf{U}}}\right)\right]\Delta^i\overline{\mathbf{U}} = -\Delta\xi\left(\frac{\partial\overline{\mathbf{F}}}{\partial\eta}\right) - \Delta^i{}_e\overline{\mathbf{P}} \tag{6}$$

where,

$$\Delta^i\overline{\mathbf{U}} = \overline{\mathbf{U}}^{i+1} - \overline{\mathbf{U}}^i, \text{ and } \overline{\mathbf{U}} = \left(\tfrac{1}{J}\right)[\rho,\ \rho u,\ \rho v,\ \rho w,\ \bar{e}]^T.$$

The superscript $i$ refers to the station $\xi = i\,\Delta\,\xi$, the values at $i+1$ being unknown. The inviscid and viscous 5x5 Jacobians, i.e. $\frac{\partial\overline{\mathbf{E}}^*}{\partial\overline{\mathbf{U}}}$, and $\frac{\partial\overline{\mathbf{F}}}{\partial\overline{\mathbf{U}}}$ are given in full in reference [14] and are not repeated here but it should be pointed out that the assumption that $\mu$ is independent of vector $\overline{\mathbf{U}}$ made in [14] is not made here.

The ISPNS code developed here belong to the class of implicit schemes which use central differencing for modelling of the fluxes. These schemes tend to introduce errors when there are discontinuities, such as shock waves in the flowfield. In order to stabilize the computer code some artificial dissipation is required which could reduce the accuracy of the ISPNS equations. Hence, to try to minimise the smoothing or artificial viscosity a box scheme has been used which is naturally dissipative together with an implicit boundary conditions (the usual no slip and zero normal pressure gradients applied at the wall) *compatible* with the finite-difference scheme used on the mesh interior. For more details of the numerical scheme and for further references on the PNS equations, see references [15] and [16].

## 4. Definition of cross-flow Reynolds number

When a wing is swept back by an angle $\Lambda$, as shown in the figure 3, the streamlines just outside the boundary layer become highly curved in planes drawn parallel to the surface. The local flow angle is

$$\phi = \tan^{-1}\left(\frac{w_e}{u_e}\right) = \tan^{-1}\left(\frac{w_\infty}{u_e}\right). \tag{7}$$

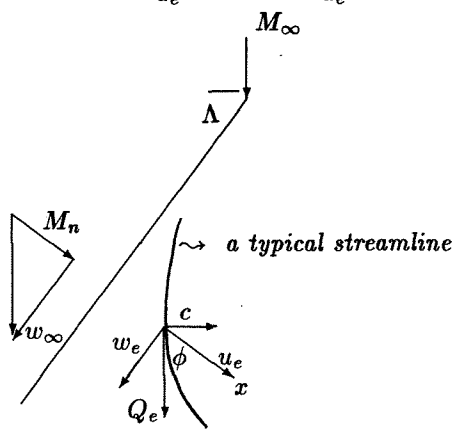


Figure 3: Supersonic flow over a swept flat-plate.

If the spanwise and the chordwise boundary-layer profiles are known, the resulting three-dimensional boundary-layer can be resolved in both cross-flow and streamwise directions. The velocity in the cross-flow direction is given by

$$c = u\sin\phi - w\cos\phi. \tag{8}$$

A characteristic Reynolds number can then be computed based on the maximum cross-flow velocity $c_{max}$

and a measure of local boundary layer thickness such as the value of $z$ at which the cross-flow velocity drops to 1% of its maximum,

$$\chi = \frac{\tilde{c}_{max}\ \tilde{\delta}_{0.01c_{max}}}{\tilde{\nu}_e}. \qquad (9)$$

Alternatively a cross-flow displacement thickness can be defined by $\delta^*_{cf}$ such that

$$\delta^*_{cf} = \int_0^e \frac{\rho c}{\rho_e c_{max}} d\tilde{y} \qquad (10)$$

and a corresponding Reynolds number by

$$Re_c = \frac{\tilde{c}_{max}\ \tilde{\delta}^*_{cf}}{\tilde{\nu}_e} = \frac{Re_n}{\mu_e}\int_0^e \rho c dy \qquad (11)$$

where the equations are non-dimensionalized with the normal to the leading edge free-stream values.

It should be noted that both definitions, Eqns (9) and (11), produce qualitatively similar results. However the $\chi$ values are usually an order of magnitude larger than $Re_c$ due to differences in the thickness ($\delta$) of the secondary profile. It was also found that the second definition, $Re_c$, produces smoother results from the integration of the boundary layer profiles whereas the other definition requires both the value of $c_{max}$ and the height above the wall where $c$ tends to 1% of $c_{max}$ which may lead to inaccuracies when they are obtained from the highly clustered grid used in the CFD code.

### 4.1 Historical background to correlation parameters

During the past 40 years there have been a number of attempts to correlate the experimentally observed transition data with particular boundary-layer parameters such as a Reynolds number, $\chi$, based on cross-flow profiles. Owen and Randall[8] have suggested a value of 125 for the onset of instability, corrected to 150 for the appearances of streaks and 200 for transition[4]. However, it has become clear that a single value of $\chi$ does not correlate all the available experimental transition data due to cross-flow instability. In practice, two or more parameters are needed. Pfenniger[3] used a cross-flow shape factor, $H_{cf} = y_{max}/\delta_{10}$, and cross-flow Reynolds number, $w_{max}\delta_{10}/\nu_e$, in the design of supercritical aerofoils whilst Arnal et al[9] identified the streamwise shape factor $H_{11}$ and $Re_c$ as suitable parameters. Better results were obtained using these correlations (C1) for a number of low speed experiments where transitional $Re_c$ varied from 50 to 150. In order to reduce the scatter in the C1 curve, Arnal et al produced a second correlation, C2, where the disturbance wave propagation direction apart from pure cross-flow direction is taken into account. This method produced better agreement with experimental results when the free-stream turbulence level is taken into account. However, the computation is expensive as $\phi$ is not known at *priori*.

For supersonic flows, where compressibility and heat transfer are important, Chapman[10] reported that using cross-flow Reynolds number correlates well with transition location. However, Chapman's cross-flow induced transition correlation is erroneous due to the fact that the transition data used in the correlation was the result of attachment line contamination, which was unknown at that time[4]. Based on yawed cone experiments, King[11] found that there was no correlation with the traditional cross-flow Reynolds number. However, he was able to produce a criterion which included both compressibility and yawed cone geometry effects. By virtue of its formulation the criterion is limited in its applicability to general geometries. More recently Reed and Haynes[12] have attempted to remedy this problem and produced a criterion which is applicable to a variety of body geometries and a wide range of flow conditions. A new cross-flow Reynolds number, corrected for compressibility and heat transfer and a shape factor similar to Pfenninger, were used to correlate transition data for spinning-cones. Their correlation appears to work well for predicting the transition location on two different yawed cone models under various angle-of-attack conditions. However, the range of validity of their criterion is limited to $2\% < w_{max}/Q_e < 8\%$, and therefore is not universally applicable, as for example, the case of a rotating disk where $w_{max}/Q_e$ is higher. Readers should be aware that Reed's compressibility and heat transfer correction factors are derived from flat plate relations where axial pressure gradients are zero. It may therefore be applied with care to similar geometries where strong pressure gradients do not exist, such as a slender cone. It should be noted that most of the high speed stability research has been done for two-dimensional and axisymmetric supersonic boundary layers. It is surprising that little research has been done applicable to high speed vehicles which are characterised by highly swept wings and three-dimensional boundary layers.

## 5. Numerical test cases

The test conditions used here closely represent the experimental conditions obtained in the Imperial College gun-tunnel:

$M_\infty = 8.8$ ; $Re_{\infty 1}$/m$= 52 * 10^6$ ; $Re_{\infty 2}$/m$= 15 * 10^6$ ;
$\tilde{L} = 7.256\text{x}10^{-2} m$ (typical chord of the delta wing tested);
$\tilde{R}_{LE} = 0.0$ and 0.4 mm, $\alpha = 0°$ and 2°;
$\Lambda = 50°$, 60° and 70° (60° delta wing, yawed 10° to the free stream;
$\tilde{T}_\infty = 64.3$ K ; $\tilde{T}_{wall} = 300.0$ K.

## 6. Discussion

### 6.1 General comments

The present ISPNS program has evolved from a previous code which has been extensively used and validated[15,16]. It has been shown that for bodies with sharp leading edges, an accurate initial condition is not required because of the parabolic nature of the equations[17]. For this reason, the initial conditions may be obtained by assuming that the flow is locally conical near the leading edge and by using a "step-back" procedure[18]. However, here the computation was started with a very small step size of $10^{-9}$ which was gradually increased to $10^{-3}$ at about $\xi = 0.01$. After this station the step size was kept constant. The code was run double-precision. For most engineering purposes it is adequate to define the boundary-layer by between 30 and 40 points. However, great care had to be taken here to compute the cross-flow profiles as they are obtained by the difference between the velocity profiles in the chordwise and spanwise directions which can be vastly different in magnitude and after resolution become of the same order of magnitude so that any errors in the solution become relatively important. Since the ISPNS code is very efficient and does not require a great deal of CPU time, 1000 points were used in the normal to the wall direction. The grid points were clustered so that at least 100 points were inside the boundary-layer. The first cell had typical heights of 1-1.5x$10^{-4}$.

### 6.2 Effects of sweep, zero incidence.

The variation of maximum cross-flow velocity, $C_{max}$, with sweep angle in the chordwise direction (normal to leading edge) is shown in figure 5. The maximum $C_{max}$ occurs near the leading edge and subsequently drops towards a limiting value. The cross-flow velocities increase monotonically with sweep due to increase in the streamline deflection angles, but the Mach number normal to the leading edge becomes less. The experimental[19] onsets of transition are marked on this graph. The maximum cross-flow velocity (normalized by the local inviscid flow), $\beta$, varies between 0.5 to 1.5% suggesting that any correlation would be outside Reed's database. This will be the subject of further study. Near the leading edge the boundary-layer is relatively thin and therefore the computed cross-flow Reynolds numbers are small. Figure 6 shows the variation of $Re_c$ obtained for a range of sweep angles as a function of surface distance normal to leading edge. In the strong interaction region, there is an initial sharp rise of $Re_c$, which increases monotonically with sweep up to 75 degrees. However, this rapid rise is followed by a gentler monotonic rise towards a maximum value in the weak interaction region. The cross-flow Reynolds numbers obtained are smaller (2-3 times) than those obtained for blunt bodies which were quoted above. The laminar to turbulent transition occurs in the weak-interation region. As shown in figure 7, the maximum value of $Re_c$ increases almost linearly with the tangent of sweep angle. However, it is not expected that $Re_c$ will continue to rise unbounded. As the sweep angle approaches 90°, $Re_c$ should fall towards zero. However, it is rather difficult to carry out the numerical analysis for sweep angles larger than 80° as the Mach number normal to the leading edge becomes subsonic and stream lines deflections also become prohibitively large. The infinite sweep assumption is unlikely to be appropriate. It is also evident from figure 6 that the cross flow Reynolds number is insensitive to the variation of the free-stream unit Reynolds number. This is not a surprising result for a sharp flat plate since, due to its geometrical similarity, the problem does not involve any streamwise length scale in the solution. The differences obtained are due to the level of numerical accuracy in the strong-interaction region. The lower unit Reynolds number results are thought to be more accurate since in these cases the initial portion of the shock and boundary layer interaction are better resolved. For example, the peak in $\beta$ ( $= c_{max}/Q_e$) near the leading edge is clearly resolved indicating larger values of $\beta$ when the free stream unit Reynolds number is lower. The transition point for a sweep angle of 70°, marked by * on figure 5, has moved downstream, suggesting a constant value for transitional Reynolds number based on local edge values and $x$, although the cross-flow Reynolds number, $Re_c$, is almost independent of $\overline{Re}_\infty$. Pure cross-flow instability can therefore not be solely responsible for the transition. Evidently, the level and the effects of free-stream noise and turbulence must be taken into account before the experimental transition data can be seriously used in future correlations.

Nevertheless, the role of cross-flow instability must not be overlooked in the transition process. The experimental[19] positions of transition shown on figures 5 and 6 clearly indicate that the transition front moves forward as the sweep angle increases. However, as shown in figure 8, the unit Reynolds number at the edge of the boundary-layer does not exhibit any significant variations with sweep angle; as expected it decreases slightly. The shockwave at the leading edge and its boundary layer interaction has a bigger effect on compression than on temperature increase so that the ratio $\rho_e/\mu_e$ increases near the leading edge ($Q_e$ stays almost constant as the spanwise velocity, $w$, is unaffected by the leading edge shockwave). As the sweep angle increases and the leading edge shockwave becomes weaker, this ratio stays almost constant.

Typically, the space marching scheme will become unstable and fail in the presence of streamwise sepa-

ration, when the regions of subsonic flow close to the walls are not thin or when the streamwise pressure gradient in these subsonic regions is strong. However, it is possible to introduce upstream influence into the solution by manipulating the $\omega \frac{\partial p}{\partial \xi}$ term on the right hand side of Eqn (6). Results have been obtained[16] where strong streamwise interactions exist and even for flows possessing a small streamwise separation bubble. Here, the above procedure was deemed unnecessary as the interaction on the swept flat plate was found to be weak, except for very close to the leading edge region. Cross-low Reynolds number, $Re_c$, reaches a maximum in the weak-interaction region. Introducing upstream influence would change the local streamlines deflection angle only slightly, and in any case, the solution is not expected to be accurate in the immediate vicinity of the leading edge.

### 6.3 Mach number effects

To investigate the effect of Mach number on the solution, the free stream Mach number was increased to 12. Although the leading edge shock wave becomes stronger, it was found that the variation of cross-flow Reynolds number with sweep angle is very much the same as that presented in figure 6, but the magnitude of cross-flow Reynolds number has increased considerably. Figure 7 shows magnitudes of the cross-flow at $x$=1.0 plotted against the tangent of sweep angle. At any particular sweep angle the increase of the cross-flow Reynolds number with Mach number is approximately proportional to $M_\infty^{2.5}$. Although not shown here, the actual values of $C_{max}/Q_e$ for both cases are almost the same. It is therefore concluded that the effect of changing the free-stream Mach number is mainly due to the change in the relative magnitude of the boundary-layer thickness.

### 6.4 Angle of attack considerations

When the delta wing is at an angle of attack $\alpha$, as shown in figure 4, the flow normal to the leading plane would be at an effective angle of attack, $\alpha_e$, scaled by the cosine of sweep angle ie

$$\alpha_e = \tan^{-1} \frac{\tan \alpha}{\cos \Lambda} \tag{12}$$

For this case the ISPNS code has been run as before but with the following non-dimensional free stream condition:

$$u = 1.0, w = \tan \Lambda, v = -\frac{\tan \alpha}{\cos \Lambda} \tag{13}$$

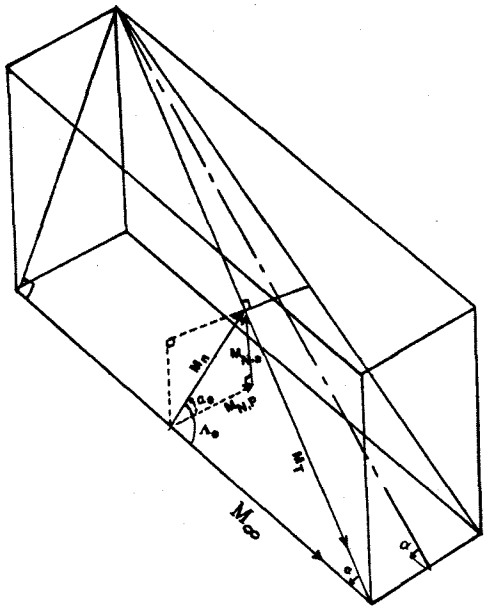

Figure 4 Schematic diagram of the flow components for the delta wing at an angle of attack.

The reference velocity is $\tilde{Q}_\infty \cos\alpha \cos\Lambda$ and the effective normal Mach number is $M_\infty \sqrt{(1.0 - \sin^2\Lambda \cos^2\alpha)}$.

Figure 8 shows the variation of cross flow Reynolds number with sweep when $\alpha$ is 2°. It can clearly be seen that magnitudes of the cross-flow Reynolds number have decreased considerably from the zero-angle of attack case. Figure 5 also indicates that the maximum cross-flow velocities have decreased for the angle of attack test case. It is therefore concluded that the streamline deflection angle reduces as $\alpha$ increases. However, the normal Mach number increases and the leading edge shock becomes stronger. Figure 9 shows the variation of unit Reynolds number, $\overline{Re}_e$ based on the boundary layer edge conditions for the two cases considered. It can be seen that, for the case with incidence, the edge unit Reynolds number is higher and, as the experimental evidence shows in figure 8, the transition has moved further forward. It is therefore concluded that the second mode of instability rather than pure cross flow is responsible for the onset of transition. As explained before, the increase in unit edge Reynolds number is due to the bigger effect on compression of the gas in comparison to an increase in its temperature at the boundary-layer edge due to the leading edge shockwave. This ratio might be expected to decrease as the sweep angle is increased due to a possible weakening of the leading edge shockwave, however the reverse is indicated on figure 9 which can be explained by examining the expression given for the effective angle of attack, $\alpha_e$ in Eqn (12). As the sweep angle increases, $\alpha_e$ also increases, causing a stronger leading edge shockwave to form, hence increasing $\overline{Re}_e$.

6.5 Wall heat transfer and code validation

The wall heat transfer for different test cases has been computed in terms of the Stanton number, St, defined by

$$St = \frac{-\tilde{\dot{q}}_w}{\tilde{\rho}_\infty \tilde{Q}_\infty (\tilde{H}_{0\infty} - \tilde{H}_w)} \qquad (14)$$

$$= \frac{1.4 M_\infty^2 \cos^2\Lambda \cos^2\alpha \, \mu_w (\frac{\partial T}{\partial y})_w}{Re_\infty Pr(1.0 + 0.2M_\infty^2 - \frac{T_w}{T_\infty})} \; (taking \; \gamma = 1.4).$$

Figure 10a shows the distribution of Stanton number when the free-stream unit Reynolds number is 52x10$^6$/m. As expected, Stanton number and heat transfer decreases with increasing sweep angle due to a reduction in $M_{\infty,n}$ and the strength of the leading edge shockwave. In figure 10a, the solid lines give Stanton number distribution for $M_\infty = 8.8$ whereas the dashed lines give similar distributions for $M_\infty = 12.0$. For the test cases considered, there is almost free stream Mach number independency. Computational data is also compared with the experimental heat transfer data[19] converted to Stanton number distribution which may introduce up to 7% error due to uncertainty in calculating $\mu_\infty$ and $Cp_\infty$ for the cold reservoir conditions of the Imperial College gun tunnel. There is also a 2% variation in the free stream Mach number, from $M_\infty = 8.8$ to 9.0, which can introduce a 4% error in the $M_\infty^2$ term of Eqn (14). Deviations from the experimental data can be noted immediately downstream from the transition point, but otherwise the agreement between experiment and the data obtained from the ISPNS code is remarkably good. The computations indicate an almost linear behaviour of the Stanton number distribution when both axes are plotted logarithmically. There is about 7% scatter in the experimental data but in the range x/L = 0.01 to 0.7 there is good agreement with the numerical data. This would lead to the conclusion that not only is the ISPNS code validated but also the infinite swept assumption is justified.

Similar remarks apply to the results presented in figure 10b obtained for the medium Reynolds number test case. There is an excellent agreement for sweep angle of 50°, but slight over and under predictions exist for sweep angles of 60° and 70° respectively. The higher levels of Stanton numbers obtained for this test case compared with the high Reynolds number test case are due to the influence of $Re_\infty$ term in the denominator of the Stanton number definition. Otherwise, the actual heat transfer rates are expected to be at least three times smaller for the medium Reynolds number test case. Figure 10c shows that the heat transfer, and therefore Stanton number, increases when the delta wing is at an angle of attack, mainly due to an increase in the strength of leading edge shockwave. Otherwise, the shape of the curves are similar to the ones reported above and there is good agreement with the experimental data up to the transition point.

## 7. Concluding remarks

The knowledge of transition location and its implications on heat transfer, drag and trim characteristics are vital in the design of swept wing aerospace planes such as HSCT aircraft. The results of the present paper are summarized in the following statements:

- It is important to verify and distinguish between the sources of transition eg. the attachment-line contamination, cross-flow instability, Görtler or T-S instability.

- High-speed flows over swept-wings with sharp leading edges lead to generation of a shock wave which in turn produces a pressure gradient behind it. The edge unit Reynolds number, $\overline{Re}_e$, is a maximum near the leading edge and subsequently decreases towards its free-stream value. Increasing the sweep decreases the shock wave strength but,

  - the $\overline{Re}_e$ varies only slightly with $\Lambda$; it decreases.
  - the combined effect of the pressure gradient and $\Lambda$ causes a generation of a cross- flow in the viscous layer which can lead to instabilities. The cross-flow Reynolds number, $Re_c$, increases with sweep angle and is shown to reach a maximum in the region of *weak interaction.*

    - $Re_c$ increases almost linearly with $\tan\Lambda$ up to $\Lambda = 80°$.
    - transition front moves forward (experimentally observed).
    - $Re_c$ increases almost as $M_\infty^{2.5}$ but is independent of $\overline{Re}_\infty$.

The last statement may have major implication for aero-space planes that rely on the upper atmosphere for re-laminarisation.

- Angle of attack, $\alpha$, reduces the production of cross-flows and $Re_c$ mainly due to a reduction in streamline deflection angle, $\phi$.

  - The strength of leading edge shock is increased which also increases $\overline{Re}_e$.
  - The variation of $\overline{Re}_e$ with $\Lambda$ is small but is increasing! as the effective $\alpha$ increases with sweep, which implies a stronger leading edge shock wave.
  - Experimental observations indicate that transition front moves forward.

## Acknowledgement

This work was partially supported by ESA (ESTEC), TRP hypersonic group, under a contract to Flow Science Ltd., Manchester.

## References

1. Smith, B.A., "F-16 XL flights could aid in HSCT design", *Aviation & Space Technology*, McGraw Hill, pp. 42-44, October 1995.

2. Hefner, J.N., "Dragging down fuel costs", *Aerospace America*, pp. 14-27, Jan 1988.

3. Pfenninger, W., "Laminar flow control-laminarisation", *Special Course on Concepts for Drag Reduction*, AGARD-R-654, pp. 3.1-3.75, March 1977.

4. Poll, D.I.A., "Transition description and prediction in three-dimensional flows", AGARD-R-709, June 1984.

5. Poll, D.I.A., "Some observations of the transition process on the windward face of a yawed cylinder", Journal of Fluid Mechanics, Vol. **150**, pp. 392-356, Jan 1985.

6. Poll, D.I.A., "A new hypothesis for transition on the windward face of space shuttle", Journal of Spacecraft and Rockets, Vol. **23**, No. 6, November 1986.

7. Gray, W.E., "The nature of the boundary-layer flow at the nose of a swept wing", RAE TM Aero 256, 1952.

8. Owen, P.R., Randall, D.S., "Boundary layer transition on the swept wing", RAE TM Aero 277, 1952.

9. Arnal, D., Habiballah, M. and Coustols, E., "Laminar instability theory and transition criteria in two and three-dimensional flow", Rech. Aerosp. **2**, pp. 45-63, 1984.

10. Chapman, G.T., "Some effects of leading edge sweep on boundary-layer transition at supersonic speeds", NASA TN D-1075, 1961.

11. King, R.A., "Three-dimensional boundary layer transition on a cone at Mach 3.5", Experiments in Fluids, Vol. **13**, 1992.

12. Reed, H.L. and Haynes, T.S., "Transition correlations in 3-D boundary layers", AIAA 93-3054, July 1993.

13. Vigneron, Y.C., Rakich, J.V. and Tannehill, J.C., "Calculations for supersonic flows over delta wings with sharp leading edges", AIAA paper 78-1137, 1978.

14. Tannehill, J.C., Venkatapathy, E. and Rakich, J.V., "Numerical solution of supersonic viscous flow over blunt delta wings", AIAA Journal, vol. **20**, No. 2, 1982.

15. Shahpar, S., and Hall, I.M., "Numerical study of hypersonic viscous cone flow", Proc. Workshop Hypersonic flows for the re-entry problems, Antibes, France, 1990 (unpublished).

16. Shahpar, S., "An Implicit Space Marching Method for High Speed Flows with Viscous-Inviscid Interactions", Proc. ICCME, Shiraz, 1993. Also published at IJST, Vol. **18**, No. 3, 1994.

17. Rudman, S. and Rubin, S.G., "Hypersonic viscous flow over slender bodies with sharp leading edges", AIAA Journal, Vol. **6**, No. 10, 1968.

18. Schiff, L.B. and Steger, J.L., "Numerical simulation of steady supersonic flow", AIAA-79-0130, 1979.

19. Hillier, R., Soltani, S. and Zanchetta, M., "Hypersonic Transition on a delta wing", Final report submitted to Flow Science Ltd., Manchester, Dec. 1995.

**Table 1 Summary of the numerical results**

| | $\Lambda$ | 40° | | 50° | | 60° | | 70° | | 75° | |
|---|---|---|---|---|---|---|---|---|---|---|---|
| | $\tan\Lambda$ | 0.839 | | 1.192 | | 1.732 | | 2.748 | | 3.732 | |
| | | tran$^\star$ | end | tran$^\star$ | end | tran$^\star$ | end | tran$^\star$ | end | tran$^\star$ | end |
| | x/L$^\dagger$ | *Lam.* | 1.000 | 0.689 | 1.000 | 0.482 | 1.000 | 0.207 | 1.000 | — | 1.000 |
| $Re_\infty = \frac{52*10^6}{m}$ $\alpha = 0°$ $M_\infty = 8.80$ | $Re_c$ | — | 18.37 | 24.95 | 25.18 | 33.30 | 34.14 | 42.49 | 46.66 | — | 57.60 |
| | $\beta/10^{-2}$ | — | 0.278 | 0.422 | 0.351 | 0.596 | 0.421 | 0.952 | 0.468 | — | 0.491 |
| | $Re_{e,x}/10^6$ | — | 3.794 | 2.619 | 3.794 | 1.837 | 3.795 | 0.793 | 3.796 | — | 3.801 |
| | $\chi$ | — | 181.6 | 247.3 | 249.6 | 332.1 | 339.8 | 422.2 | 458.1 | — | 553.4 |
| | x/L$^\dagger$ | *Lam.* | 1.000 | *Lam.* | 1.000 | *Lam.* | 1.000 | 0.689 | 1.000 | — | 1.000 |
| $Re_\infty = \frac{15*10^6}{m}$ $\alpha = 0°$ $M_\infty = 8.80$ | $Re_c$ | — | 17.93 | — | 24.63 | — | 33.60 | 48.66 | 49.23 | — | 56.66 |
| | $\beta/10^{-2}$ | — | 0.506 | — | 0.637 | — | 0.766 | 1.092 | 0.916 | — | 0.884 |
| | $Re_{e,x}/10^6$ | — | 1.099 | — | 1.909 | — | 1.099 | 0.761 | 1.101 | — | 1.103 |
| | $\chi$ | — | 173.0 | — | 239.1 | — | 327.6 | 470.2 | 476.1 | — | 527.4 |
| | x/L$^\dagger$ | — | 1.000 | 0.551 | 1.000 | 0.345 | 1.000 | 0.165 | 1.000 | — | 1.000 |
| $Re_\infty = \frac{52*10^6}{m}$ $\alpha = 2°$ $M_\infty = 8.80$ | $Re_c$ | — | 12.72 | 16.66 | 17.02 | 22.00 | 23.05 | 27.14 | 31.56 | — | 40.16 |
| | $\beta/10^{-2}$ | — | 0.166 | 0.289 | 0.209 | 0.426 | 0.244 | 0.642 | 0.265 | — | 0.300 |
| | $Re_{e,x}/10^6$ | — | 4.349 | 2.399 | 4.354 | 1.505 | 4.368 | 0.732 | 4.404 | — | 4.462 |
| | $\chi$ | — | 95.93 | 135.5 | 132.8 | 181.3 | 175.4 | 228.4 | 232.7 | — | 305.4 |

$\star$ experimentally observed[19]

† L=72.5589 cm

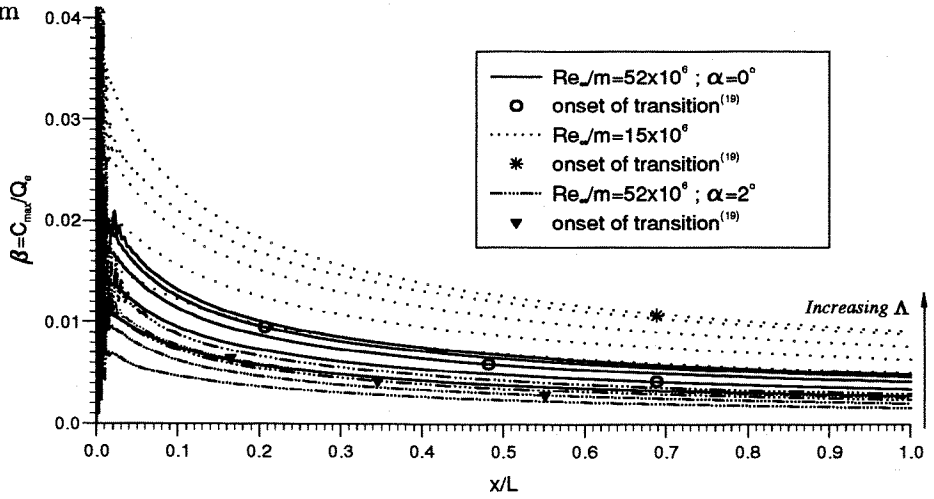


Fig 5. Variation of maximum cross-flow velocity with sweep angle and free-stream unit Reynolds number

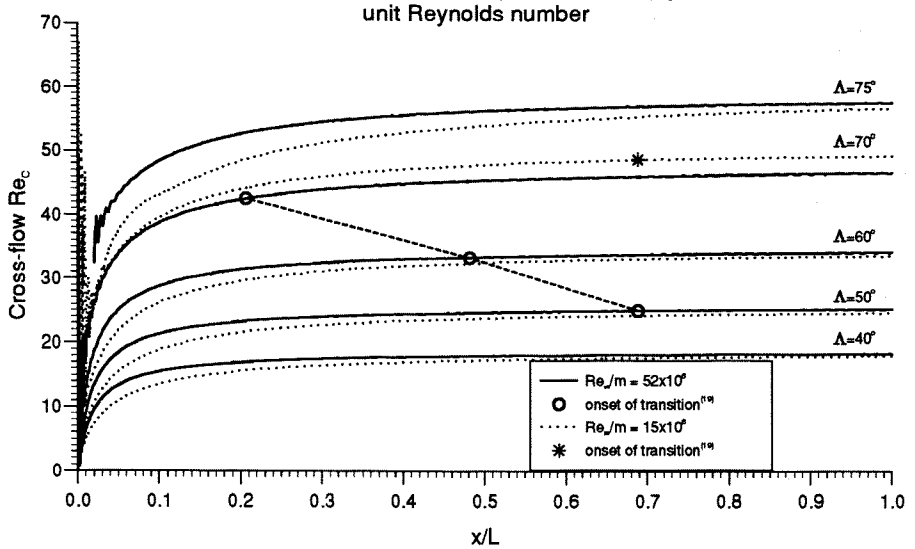


Fig 6. Variation of cross-flow Reynolds number with sweep angle and free-stream unit Reynolds number

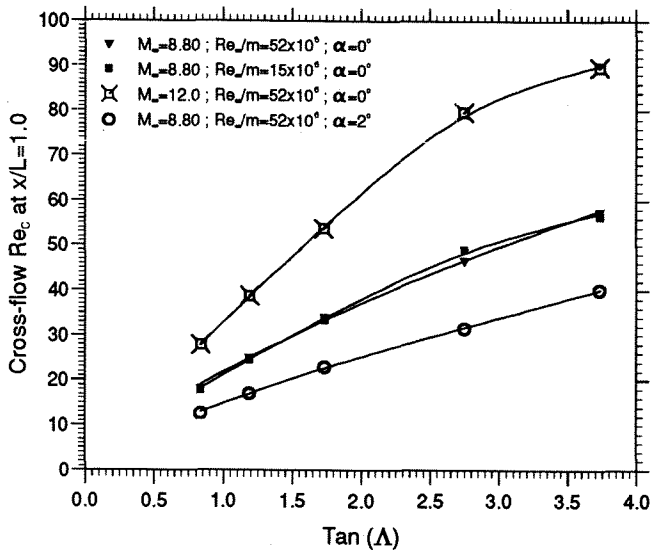


Fig 7. Variation of cross-flow Reynolds number with $M_\infty$, $\Lambda$, unit $Re_\infty$ and angle of attack ($\alpha$).

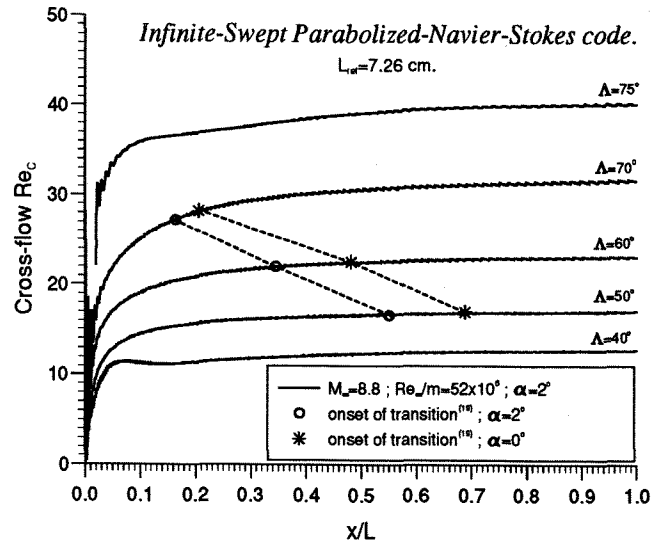


Fig 8. Variation of cross-flow Reynolds number with sweep angle for the angle of attack test case.

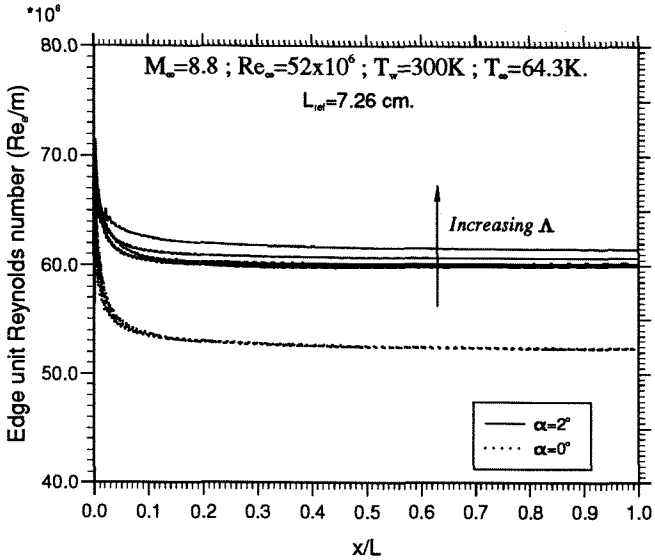


Fig 9. Variation of edge unit Reynolds number with sweep angle and angle of attack, $\alpha$.

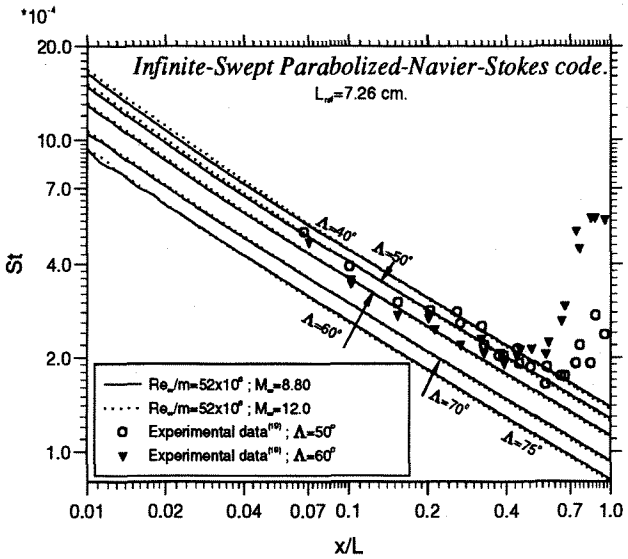


Fig 10a. Variation of Stanton number with sweep angle and free-stream Mach number.

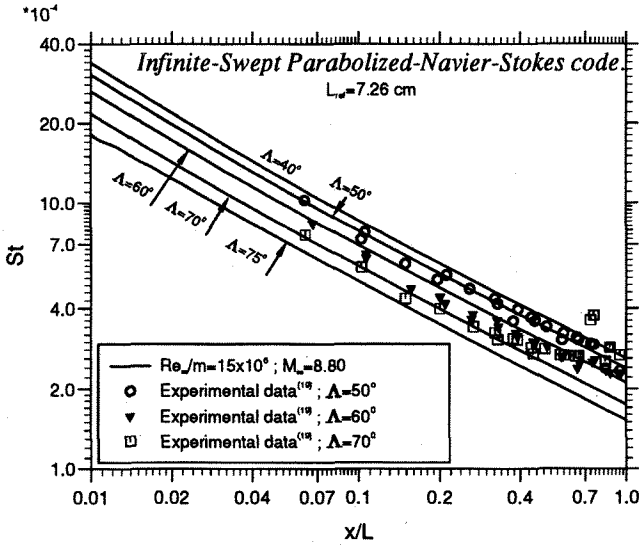


Fig 10b. Variation of Stanton number with sweep angle for the medium Reynolds number test case.

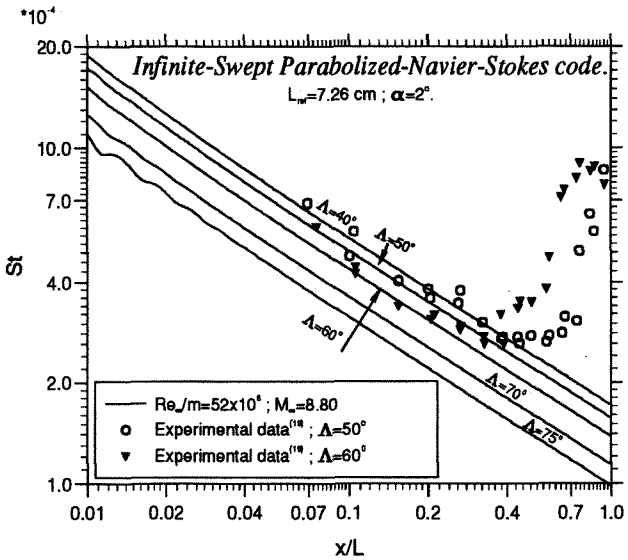


Fig 10c. Variation of Stanton number with sweep angle for the angle of attack test case.